

Resistive anisotropy due to spin-fluctuation scattering in the nematic phase of iron pnictides

Maxim Breitkreuz,^{1,*} P. M. R. Brydon,² and Carsten Timm^{1,†}

¹*Institute of Theoretical Physics, Technische Universität Dresden, 01062 Dresden, Germany*

²*Condensed Matter Theory Center, Department of Physics, University of Maryland, College Park, Maryland 20742, USA*

(Received 4 June 2014; revised manuscript received 29 August 2014; published 10 September 2014)

The large in-plane anisotropy of the resistivity is a hallmark of the nematic state of the iron pnictides. Solving the Boltzmann transport equation, we show that the prominent doping dependence as well as the large values of the anisotropy can be well explained by momentum-dependent spin-fluctuation scattering without assuming anisotropic impurity states. Due to the forward-scattering corrections, the hot spots contribute to the resistive anisotropy even in the case of strong spin fluctuations, which makes large values of the anisotropy possible. The ellipticity of the electron pockets plays an important role in explaining the dominance of positive values of the anisotropy, i.e., larger resistivity in the direction with weaker spin fluctuations, throughout the doping range.

DOI: [10.1103/PhysRevB.90.121104](https://doi.org/10.1103/PhysRevB.90.121104)

PACS number(s): 72.10.Di, 72.15.Lh, 74.70.Xa

Introduction. Currently, one of the most intensively discussed topics in the field of high- T_c superconductivity is the origin of the nematic phase of the iron pnictides [1,2]. The nematic phase transition occurs at temperatures T_s above or coinciding with the magnetic ordering temperature T_N , at which a stripe antiferromagnetic state with ordering vector $\mathbf{Q}_X = (\pi, 0)$ (defining the x direction in this work) is established. The nematic phase found for $T_N < T < T_s$ is characterized by a broken rotational symmetry between the x and y directions in the absence of magnetic order. Although one of its most obvious manifestations is the orthorhombic distortion of the lattice, it is generally considered that the nematic state arises from electronic correlations [3]. However, the precise mechanism is still under debate [4–8].

Another key experimental signature of the nematic phase is the pronounced difference between the resistivities along the x and y directions, $\Delta\rho \equiv (\rho_y - \rho_x)/\rho_x$ [3,9–12]. Understanding the origin of the resistive anisotropy should offer crucial insights into the origin of the nematicity. Two scenarios are debated: (i) the scattering off anisotropic impurity states [9,13–16] and (ii) the scattering off fluctuating collective excitations with spectrum reflecting the underlying nematicity [11,17].

The existing description of the resistive anisotropy due to spin fluctuations [17], i.e., within scenario (ii), is restricted to the limit of weak spin-fluctuation scattering compared to isotropic impurity scattering, although the former is likely stronger than the latter, except at very low temperatures when the spin fluctuations are frozen out [18–22]. Naturally, this limit is only compatible with small values of $\Delta\rho$, since the dominant impurity part leads to isotropic resistivity. Though in disagreement with the huge positive anisotropy up to $\Delta\rho \approx 0.5$ observed in experiments on electron-doped samples [3,9], the theory correctly predicts negative $\Delta\rho$ for hole-doped samples [11].

Within scenario (i), the much larger $\Delta\rho$ in electron-doped $\text{Ba}(\text{Fe}_{1-x}\text{Co}_x)_2\text{As}_2$ [3] compared to hole-doped $\text{Ba}_{1-x}\text{K}_x\text{Fe}_2\text{As}_2$ [11,12] is explained as a consequence of the stronger scattering off Co dopants placed *within* the iron plane [9,13,16]. The observed anisotropic impurity states are

all elongated in the x direction, hence giving a larger scattering cross section in the y direction [13]. The negative $\Delta\rho$ measured for hole-doped samples then arises due to details of the band structure [16]. The dependence of $\Delta\rho$ on the degree of disorder is controversial: some experiments show, in agreement with scenario (i), a reduction of $\Delta\rho$ upon sample annealing, which is supposed to lower the degree of disorder [9], while others report a much weaker disorder dependence [10].

In this work, we consider scenario (ii) with spin-fluctuation scattering of arbitrary strength. For spin-fluctuation and isotropic impurity scattering of comparable strength, we reproduce both the small negative $\Delta\rho$ for hole-doped samples and the large positive $\Delta\rho$ in electron-doped samples. We also show that the reduction of $\Delta\rho$ in electron-doped samples upon annealing is consistent with the spin-fluctuation scenario. In a nutshell, our results follow from the role of the spin-fluctuation scattering strength in controlling the size of the Fermi-surface segments that contribute to the resistive anisotropy.

Model and method. We describe the band structure by an effective two-dimensional model [5,11,17,22,23] with a nearly circular hole Fermi pocket at the center of the Brillouin zone and two elliptical electron pockets eX and eY displaced by $\mathbf{Q}_X = (\pi, 0)$ and $\mathbf{Q}_Y = (0, \pi)$, respectively, where length is measured in units of the iron-iron separation. We use the same dispersions as in Ref. [23] and fix the ellipticity of the electron pockets by choosing $\xi_e = 2$. The Fermi pockets are sketched in Fig. 1. The sizes of the pockets depend on the doping level, which is controlled by the electron filling n [22]. The validity of the minimal model for the case of 122 pnictides has been discussed in the supplementary information for Ref. [11].

To focus on the impact of the spin-fluctuation scattering, in the following we neglect the distortion of the Fermi pockets due to the splitting of the iron d_{yz} and d_{xz} orbital levels [24,25]. In the Supplemental Material [26] we show that this splitting gives rise to an additional resistive anisotropy. By itself, this shows poor agreement with experiment, however, and the effect of nematicity in the spin-fluctuation scattering is the dominant mechanism over a large parameter range.

We assume transport to be dominated by scattering off spin fluctuations and isotropic impurities. The spin-fluctuation scattering amplitude is determined by the imaginary part of the spin susceptibility. We use a phenomenological model for the susceptibility in the nematic phase that has been employed

*maxim.breitkreuz@tu-dresden.de

†carsten.timm@tu-dresden.de

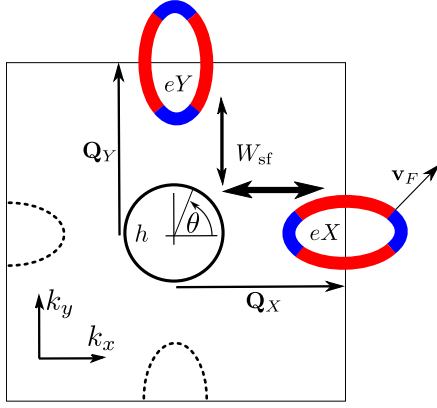


FIG. 1. (Color online) Hole (h) and electron (eX and eY) Fermi pockets of the two-band model. In the nematic phase, scattering between h and eX is stronger than between h and eY , as indicated by the arrows marked W_{sf} , giving rise to the resistive anisotropy. As discussed in the main text, the electron pockets can be divided into regions that contribute positively (red) or negatively (blue) to the anisotropy, depending on the direction of the Fermi velocity. States on each Fermi surface are parametrized by the angle θ to the x axis with respect to the center of the pocket.

for calculations in the impurity-dominated regime [17,27,28]. Following Ref. [22], we introduce a total elastic scattering rate between states $|s, \theta\rangle$ on the Fermi pockets, parametrized by the pocket index s and the angle θ (cf. Fig. 1),

$$W_{s\theta}^{s'\theta'} \equiv (1 - \delta_{bb'}) W_{sf} \alpha \times \int d\varepsilon' \varepsilon' \frac{\coth \frac{\varepsilon'}{2k_B T} - \tanh \frac{\varepsilon'}{2k_B T}}{\varepsilon'^2 + \omega_{\mathbf{q}}^2} + W_{imp}, \quad (1)$$

where $\omega_{\mathbf{q}} = \Gamma(\xi^{-2} \mp \phi + q_x^2(1 \pm \eta) + q_y^2(1 \mp \eta))$ with $\mathbf{q} = \mathbf{k}(s, \theta, \varepsilon_F) - \mathbf{k}(s', \theta', \varepsilon')$, where the wave vectors are measured from the center of the corresponding Fermi pocket. Further, b (b') is the band giving rise to the Fermi pocket s (s'), ϕ is the nematic order parameter, ξ is the correlation length in the isotropic phase, Γ is the Landau damping parameter, and η is the in-plane anisotropy of the correlation length. The upper (lower) sign corresponds to the scattering between the hole pocket and the electron pocket eX (eY). W_{sf} and W_{imp} represent the overall strengths of the scattering off spin fluctuations and impurities, respectively, and the numerical factor $\alpha = 10$ ensures that at the highest considered temperature (see below) W_{sf}/W_{imp} is of the same order as the inverse ratio of average lifetimes due to scattering off spin fluctuations and impurities only, $W_{sf}/W_{imp} \sim \tau_{imp}/\tau_{sf}$.

The susceptibility entering Eq. (1) is peaked at the nesting vectors \mathbf{Q}_X and \mathbf{Q}_Y for all dopings, consistent with the observed stability of commensurate antiferromagnetic order against doping. The resulting scattering rate is therefore larger for scattering wave vectors close to \mathbf{Q}_X or \mathbf{Q}_Y . The strongest scattering is found at the ‘‘hot spots,’’ i.e., the points on the Fermi pockets connected by the nesting vectors. The position of the hot spots depends on the doping level [22,23]. In the nematic phase a finite order parameter $\phi > 0$ breaks the C_4 symmetry. This enhances the peak at \mathbf{Q}_X in the susceptibility, leading to stronger scattering between the hole pocket h and

the electron pocket eX than between the pockets h and eY , as indicated in Fig. 1.

We focus on the dependence of the resistive anisotropy on doping (electron filling n) and on the relative strengths of spin-fluctuation and impurity scattering (controlled by W_{sf}/W_{imp}). The explicit temperature T in Eq. (1) controls the energy available for spin excitations and thus additionally affects the strength of spin-fluctuation scattering. In the relevant limit $k_B T \ll \omega_{\mathbf{q}}$, this leads to the familiar T^2 dependence. Since the nematic phase appears in a narrow temperature interval above the Néel temperature $T_N(n)$, we choose the temperature $T(n) = T_N(n) = T_0\{1 - [(n - 2.09)/0.2]^2\}$ with $T_0 = \max[T_N(n)] = 137$ K. This mimics the situation in 122 pnictides, where the magnetic order is suppressed upon doping the parent compound, here taken to correspond to $n = 2.09$ [23]. Our results are qualitatively insensitive to the specific form of $T(n)$. Since the temperature tracks $T_N(n)$, it is reasonable to keep the parameters ξ , ϕ , and Γ fixed; we have checked that the qualitative behavior does not depend on their precise values.

We employ the nonequilibrium Green’s function formalism [29] in the Boltzmann approximation, where the linear-response distribution function at the Fermi energy is determined by the vector mean free paths $\Lambda_{s\theta}$ [30,31] of the states $|s, \theta\rangle$. The vector mean free path obeys the kinetic equation [22]

$$\Lambda_{s\theta} = \tau_{s\theta} \mathbf{v}_{s\theta} + \tau_{s\theta} \sum_{s'} \int \frac{d\theta'}{2\pi} N_{s'\theta'} W_{s\theta}^{s'\theta'} \Lambda_{s'\theta'}, \quad (2)$$

where $\mathbf{v}_{s\theta} \equiv \hbar^{-1} \nabla_{\mathbf{k}} \varepsilon_{b\mathbf{k}}|_{s, \theta}$ is the velocity, $N_{s\theta} = |d\mathbf{k}_{s\theta}/d\theta|/\pi\hbar|\mathbf{v}_{s\theta}|$ is the density of states, and

$$\tau_{s\theta} = \left(\frac{1}{2\pi} \sum_{s'} \int d\theta' N_{s'\theta'} W_{s\theta}^{s'\theta'} \right)^{-1} \quad (3)$$

is the lifetime of the state $|s, \theta\rangle$. The first term on the right-hand side of Eq. (2) represents the relaxation-time approximation, while the second incorporates the forward-scattering corrections.

The resistivity ρ_i in the direction $i = x, y$ is determined by the vector mean free path,

$$\rho_i = \left(e^2 \sum_s \int \frac{d\theta}{2\pi} N_{s\theta} v_{s\theta}^i \Lambda_{s\theta}^i \right)^{-1} \equiv \left(\sum_s \int \frac{d\theta}{2\pi} \sigma_{s\theta}^i \right)^{-1}, \quad (4)$$

where $\sigma_{s\theta}^i$ is the contribution of the state $|s, \theta\rangle$ to the total conductivity $\sigma^i = \sum_s \int \frac{d\theta}{2\pi} \sigma_{s\theta}^i$. It is useful to resolve the resistive anisotropy in terms of band and angular contributions,

$$\Delta\rho = \int \frac{d\theta}{2\pi} (\Delta\rho_{h\theta} + \Delta\rho_{e\theta}), \quad (5)$$

where the contributions from hole and electron pockets read, respectively,

$$\Delta\rho_{h\theta} \equiv \frac{1}{2\sigma^y} (\sigma_{h,\theta}^x - \sigma_{h,\theta}^y + \sigma_{h,\theta+\pi/2}^x - \sigma_{h,\theta+\pi/2}^y), \quad (6)$$

$$\Delta\rho_{e\theta} \equiv \frac{1}{\sigma^y} (\sigma_{eY,\theta}^x - \sigma_{eY,\theta}^y + \sigma_{eX,\theta+\pi/2}^x - \sigma_{eX,\theta+\pi/2}^y). \quad (7)$$

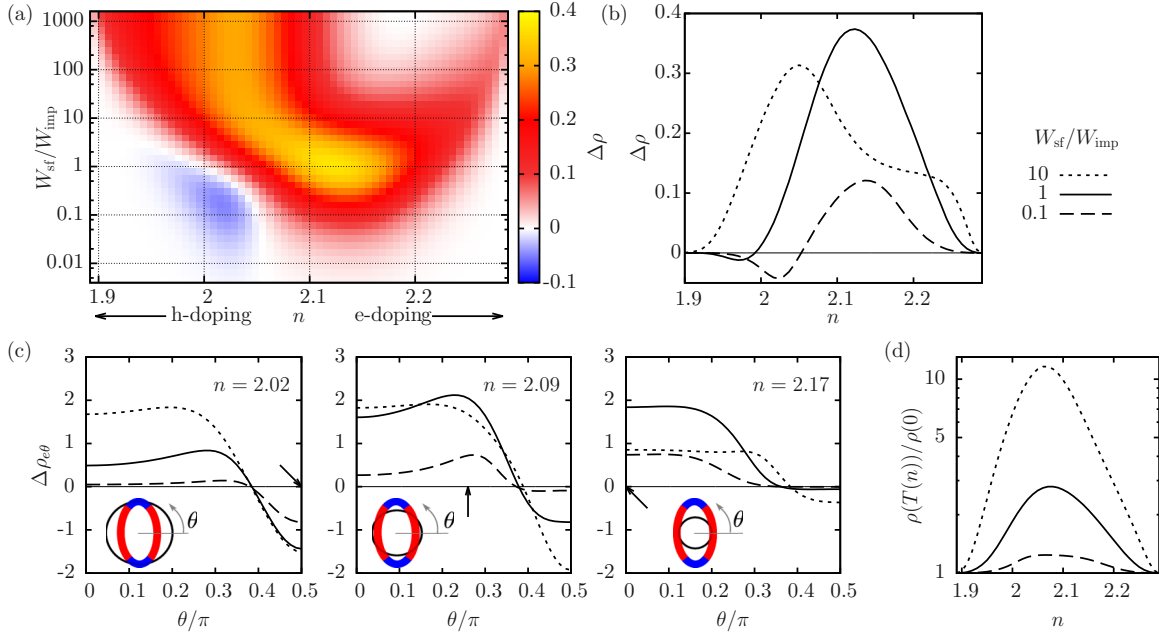


FIG. 2. (Color online) (a) Resistive anisotropy as a function of doping (parametrized by n) and the relative strengths of spin-fluctuation and impurity scattering. (b) Resistive anisotropy as a function of doping for $W_{sf}/W_{imp} = 0.1, 1,$ and 10 . (c) Angle-resolved contributions of the electron pockets to the resistive anisotropy as defined in Eq. (7). While for $W_{sf}/W_{imp} = 0.1$ only regions close to the hot spots (indicated by arrows) contribute, for increasing W_{sf}/W_{imp} the contributing regions grow. (d) Ratio of averaged resistivities at the temperatures $T(n)$ considered in (a)–(c) and at $T = 0$ K. We choose the parameters $\eta = 0.5$, $\Gamma = 350$ meV, $\xi^{-2} = 0.027$, and $\phi = 0.017$.

In Eq. (6), we consider the contributions from the hole-pocket states $|h, \theta\rangle$ and $|h, \theta + \pi/2\rangle$ together, since only the joint contribution vanishes in the normal, C_4 -symmetric phase. For the same reason, the states $|eY, \theta\rangle$ and $|eX, \theta + \pi/2\rangle$ are considered together in Eq. (7). According to the definition of $\Delta\rho_{e\theta}$, the contributions from states close to the minor axis of the elliptical electron pockets are found at $\theta \approx 0$, while the contributions from states close to the major axis are found at $\theta \approx \pi/2$.

Results. Figure 2 summarizes the results for the resistive anisotropy obtained by solving Eq. (2) numerically [22]. In Fig. 2(a) the resistive anisotropy is plotted as a function of doping and the ratio W_{sf}/W_{imp} , while in Fig. 2(b) the doping dependence is illustrated for three characteristic values of W_{sf}/W_{imp} . The contributions $\Delta\rho_{e\theta}$ from the electron pockets are found to dominate the anisotropy, for which reason only these contributions are shown in Fig. 2(c). As evident from Fig. 2(c) and illustrated in Fig. 1, the electron pockets can be divided into positively and negatively contributing parts, with the crossover located roughly where the Fermi velocity points in the diagonal direction; the parts close to the minor axis of the electron pockets contribute with positive sign, while the parts close to the major axis contribute with negative sign. This is because the conductivity of the electron pocket eY is larger than that of eX due to the stronger scattering for the latter.

The total resistive anisotropy in Figs. 2(a) and 2(b) shows a strong doping dependence, which changes qualitatively with W_{sf}/W_{imp} . The angle-resolved plots in Fig. 2(c) show that for increasing W_{sf}/W_{imp} the contributing regions of the electron pockets expand. This is schematically illustrated in Fig. 3. For small W_{sf}/W_{imp} , the resistive anisotropy is dominated by regions close to the hot spots, whereas the

“cold” regions, where spin-fluctuation scattering is weaker, give small contributions. Since the electron pockets have negatively and positively contributing parts, the position of the hot spots determines the sign of the resistive anisotropy. The negative (positive) extremum is found for the filling $n \approx 2.02$ ($n \approx 2.17$), for which the hot spots lie on the major (minor) axis of the electron pockets. The difference between the positive and negative extrema is due to different velocities and densities of states at the major and minor axes.

In the impurity-dominated limit, $W_{sf}/W_{imp} \ll 1$, the anisotropy is very small as impurity scattering is isotropic. With increasing W_{sf}/W_{imp} , the contributing regions of the electron pockets expand and the extrema of $\Delta\rho$ grow, until the active region starts to include parts contributing with

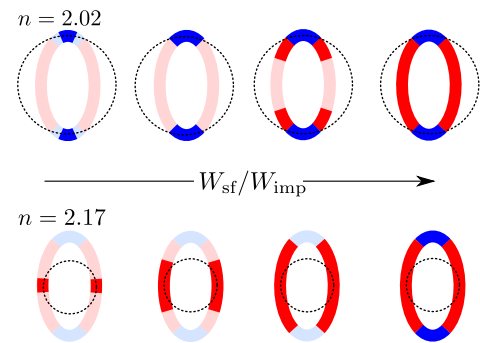


FIG. 3. (Color online) Increasing strength of spin-fluctuation scattering extends the contributing regions of the electron pockets. Two characteristic filling levels are considered, $n \approx 2.02$ and $n \approx 2.17$, with hot spots at the major and the minor axis of the electron pockets, respectively.

the opposite sign. Upon further expansion, the positive and negative contributions begin to partially compensate each other. Since the negatively contributing regions are smaller, the negative extremum of $\Delta\rho$ is suppressed at a smaller ratio W_{sf}/W_{imp} than the positive extremum. At $W_{sf}/W_{imp} \approx 1$ this results in a strong doping asymmetry with small negative values on the hole-doped side and large positive values on the electron-doped side.

We emphasize that the result that the hot spots contribute to $\Delta\rho$ even for dominant spin-fluctuation scattering, as sketched in Fig. 3, is not obvious. Since in this limit the scattering at the hot spots is much stronger than in the cold regions, one would naively expect the hot spots to be short circuited by the cold regions [32], i.e., to be irrelevant for the transport, in which case $\Delta\rho$ would be significantly smaller [11,17]. However, as we have shown for the C_4 -symmetric state of the pnictides [22], the short-circuiting is compensated by enhanced forward-scattering corrections.

To compare the results to measurements, we have to identify the relevant range of W_{sf}/W_{imp} . In Fig. 2(d), we plot the calculated ratio of the averaged resistivity $\rho(T) \equiv (\rho_x + \rho_y)/2$ at $T = T(n)$ and at $T = 0$ K, where the spin excitations are frozen out and the resistivity is due to impurity scattering alone, which we assume to be temperature independent. Ignoring for the moment that the system is antiferromagnetic at $T = 0$ K, we observe that for $W_{sf}/W_{imp} = 1$ and $W_{sf}/W_{imp} = 10$ the resistivity ratios are comparable to those measured for as-grown and annealed samples, respectively [9]. The reduction of the density of states in the antiferromagnetic phase should increase the $T = 0$ K resistivity, however, and so our argument likely underestimates W_{sf}/W_{imp} .

For $W_{sf}/W_{imp} = 1$, Figs. 2(a) and 2(b) show a large positive peak with $\Delta\rho \approx 0.4$ in electron-doped samples and a small negative peak with $\Delta\rho \approx -0.01$ in hole-doped samples. This is in good agreement with experimental observations [3,9,11]. The results also show that in electron-doped samples an increase of W_{sf}/W_{imp} beyond about 1 leads to a reduction

of the peak value of $\Delta\rho$. A reduction of $\Delta\rho$ upon annealing was indeed observed in electron-doped $\text{Ba}(\text{Fe}_{1-x}\text{Co}_x)_2\text{As}_2$ [9], where this effect has been taken as strong evidence that the resistive anisotropy mainly stems from scattering at anisotropic impurity states. Our results show, however, that such a reduction is also consistent with anisotropic spin-fluctuation scattering. For the hole-doped samples, we predict an *increase* in $\Delta\rho$ with annealing if $W_{sf}/W_{imp} \gtrsim 1$, see Figs. 2(a) and 2(b), which to our knowledge has not been measured so far.

In the Supplemental Material [26], we show that anisotropy due to orbital splitting adds nearly additively to $\Delta\rho$, indicating the robustness of the results against band details. This is in line with the fact that the main features of $\Delta\rho$ are explained by a mechanism that does not rely on the details of the model.

Summary. We have studied the resistive anisotropy in the nematic state of iron pnictides. We have considered a two-band model and assumed scattering to be dominated by spin fluctuations and isotropic impurities. The inclusion of forward-scattering corrections is crucial for the correct description [22]. The obtained resistive anisotropy $\Delta\rho$ shows good agreement with experimental results for annealed and as-grown samples. In particular, we have shown that the twin puzzles of the doping asymmetry of $\Delta\rho$ and the reduction of $\Delta\rho$ upon annealing can be explained within the spin-fluctuation scenario. The qualitative behavior is governed by the contributing regions on the elliptical electron pockets, in particular their growth with increasing spin-fluctuation strength. Importantly, the hot spots contribute to $\Delta\rho$ even for strong spin-fluctuation scattering, contrary to what was thought previously. Since spin fluctuations are particularly strong at the hot spots, this naturally leads to large anisotropies.

Acknowledgments. Financial support by the Deutsche Forschungsgemeinschaft (Germany) through Research Training Group GRK 1621 is gratefully acknowledged. The authors thank B. M. Andersen, E. Babaev, M. N. Gastiasoro, P. J. Hirschfeld, D. Inosov, and J. Schmiedt for useful discussions.

-
- [1] R. M. Fernandes, A. V. Chubukov, and J. Schmalian, *Nat. Phys.* **10**, 97 (2014).
- [2] J. C. Davis and P. J. Hirschfeld, *Nat. Phys.* **10**, 184 (2014).
- [3] J.-H. Chu, J. G. Analytis, K. De Greve, P. L. McMahon, Z. Islam, Y. Yamamoto, and I. R. Fisher, *Science* **329**, 824 (2010).
- [4] W. Lv and P. Phillips, *Phys. Rev. B* **84**, 174512 (2011).
- [5] R. M. Fernandes, A. V. Chubukov, J. Knolle, I. Eremin, and J. Schmalian, *Phys. Rev. B* **85**, 024534 (2012).
- [6] S. Onari and H. Kontani, *Phys. Rev. Lett.* **109**, 137001 (2012).
- [7] V. Stanev and P. B. Littlewood, *Phys. Rev. B* **87**, 161122 (2013).
- [8] S. Liang, A. Moreo, and E. Dagotto, *Phys. Rev. Lett.* **111**, 047004 (2013).
- [9] S. Ishida, M. Nakajima, T. Liang, K. Kihou, C. H. Lee, A. Iyo, H. Eisaki, T. Kakeshita, Y. Tomioka, T. Ito, and S. Uchida, *Phys. Rev. Lett.* **110**, 207001 (2013).
- [10] H.-H. Kuo and I. R. Fisher, *Phys. Rev. Lett.* **112**, 227001 (2014).
- [11] E. C. Blomberg, M. A. Tanatar, R. M. Fernandes, I. I. Mazin, B. Shen, H.-H. Wen, M. D. Johannes, J. Schmalian, and R. Prozorov, *Nat. Commun.* **4**, 1914 (2013).
- [12] J. J. Ying, X. F. Wang, T. Wu, Z. J. Xiang, R. H. Liu, Y. J. Yan, A. F. Wang, M. Zhang, G. J. Ye, P. Cheng, J. P. Hu, and X. H. Chen, *Phys. Rev. Lett.* **107**, 067001 (2011).
- [13] M. P. Allan, T.-M. Chuang, F. Massee, Yang Xie, Ni Ni, S. L. Bud'ko, G. S. Boebinger, Q. Wang, D. S. Dessau, P. C. Canfield, M. S. Golden, and J. C. Davis, *Nat. Phys.* **9**, 220 (2013).
- [14] Y. Inoue, Y. Yamakawa, and H. Kontani, *Phys. Rev. B* **85**, 224506 (2012).
- [15] M. N. Gastiasoro, P. J. Hirschfeld, and B. M. Andersen, *Phys. Rev. B* **89**, 100502(R) (2014).
- [16] M. N. Gastiasoro, I. Paul, Y. Wang, P. J. Hirschfeld, and B. M. Andersen, *arXiv:1407.0117*.
- [17] R. M. Fernandes, E. Abrahams, and J. Schmalian, *Phys. Rev. Lett.* **107**, 217002 (2011).
- [18] L. Fang, H. Luo, P. Cheng, Z. Wang, Y. Jia, G. Mu, B. Shen, I. I. Mazin, L. Shan, C. Ren, and H.-H. Wen, *Phys. Rev. B* **80**, 140508(R) (2009).
- [19] S. Kasahara, T. Shibauchi, K. Hashimoto, K. Ikada, S. Tonegawa, R. Okazaki, H. Shishido, H. Ikeda, H. Takeya,

- K. Hirata, T. Terashima, and Y. Matsuda, *Phys. Rev. B* **81**, 184519 (2010).
- [20] L. Fanfarillo, E. Cappelluti, C. Castellani, and L. Benfatto, *Phys. Rev. Lett.* **109**, 096402 (2012).
- [21] M. Breitzkreiz, P. M. R. Brydon, and C. Timm, *Phys. Rev. B* **88**, 085103 (2013).
- [22] M. Breitzkreiz, P. M. R. Brydon, and C. Timm, *Phys. Rev. B* **89**, 245106 (2014).
- [23] P. M. R. Brydon, J. Schmiedt, and C. Timm, *Phys. Rev. B* **84**, 214510 (2011).
- [24] M. Yi, D. Lu, J.-H. Chu, J. G. Analytis, A. P. Sorini, A. F. Kemper, B. Moritz, S.-K. Mo, M. G. Moore, M. Hashimoto, W.-S. Lee, Z. Hussain, T. P. Devereaux, I. R. Fisher, and Z.-X. Shen, *Proc. Natl. Acad. Sci. USA* **108**, 6878 (2011).
- [25] K. Nakayama, Y. Miyata, G. N. Phan, T. Sato, Y. Tanabe, T. Urata, K. Tanigaki, and T. Takahashi, [arXiv:1404.0857](https://arxiv.org/abs/1404.0857).
- [26] See Supplemental Material at <http://link.aps.org/supplemental/10.1103/PhysRevB.90.121104> for the discussion of the effect of splitting of d_{yz} and d_{xz} orbital levels on the resistive anisotropy within the present model.
- [27] D. S. Inosov, J. T. Park, P. Bourges, D. L. Sun, Y. Sidis, A. Schneidewind, K. Hradil, D. Haug, C. T. Lin, B. Keimer, and V. Hinkov, *Nat. Phys.* **6**, 178 (2010).
- [28] S. O. Diallo, D. K. Pratt, R. M. Fernandes, W. Tian, J. L. Zarestky, M. Lumsden, T. G. Perring, C. L. Broholm, N. Ni, S. L. Bud'ko, P. C. Canfield, H.-F. Li, D. Vaknin, A. Kreyssig, A. I. Goldman, and R. J. McQueeney, *Phys. Rev. B* **81**, 214407 (2010).
- [29] J. Rammer and H. Smith, *Rev. Mod. Phys.* **58**, 323 (1986).
- [30] G. D. Mahan, *Many-Particle Physics*, 3rd ed. (Plenum, New York, 2000).
- [31] E. H. Sondheimer, *Proc. R. Soc. London, Ser. A* **268**, 100 (1962); P. L. Taylor, *ibid.* **275**, 200 (1963).
- [32] R. Hlubina and T. M. Rice, *Phys. Rev. B* **51**, 9253 (1995).